ELSEVIER

J. Non-Newtonian Fluid Mech. 142 (2007) 79–94

Journal of Non-Newtonian Fluid Mechanics

www.elsevier.com/locate/jnnfm

Two-dimensional dam break flows of Herschel–Bulkley fluids: The approach to the arrested state

G.P. Matson, A.J. Hogg*

Centre for Environmental & Geophysical Flows, School of Mathematics, University of Bristol, University Walk, Clifton, Bristol. BS8 1TW, United Kingdom

Received 24 February 2006; received in revised form 5 May 2006; accepted 5 May 2006

Abstract

Dam break flows of viscoplastic fluids are studied theoretically using a Herschel–Bulkley constitutive law and a lubrication model of the motion. Following initiation these fluids are gravitationally driven out of the lock in which they had resided. Their motion is eventually arrested because they exhibit a yield stress and they attain a stationary state in which the gravitational forces are in equilibrium with the yield stress. We study the evolution of these flows from initiation to arrest by integrating the equations of motion numerically. We demonstrate that the final arrested state is approached asymptotically and find analytically that the perturbations to the final state decay algebraically with time as $1/t^n$, where n is the power index of the Herschel–Bulkley model.

Keywords: Viscoplastic fluid; Yield stress; Dam break flow; Free-surface flow; Arrested state

1. Introduction

In all manner of environmental and industrial processes, the gravitationally driven spreading of a layer of viscoplastic fluid is an important phenomenon. Examples include the flow of lava down the flank of volcanos [1,2] and the release and sliding of mud [3–6]. Relatively slow moving slumps of Newtonian, viscous fluids have received extensive study (see, for example, Huppert [7] and Lister [8]), but often in a geophysical or manufacturing context the rheology is more complicated. Fluids such as lavas, muds, liquid foods and concrete exhibit complex properties that may include a yield stress and a nonlinear relationship between shear-stress and strain-rate [9]. Incorporating a yield stress into any model is particularly challenging as a discontinuity is introduced between flowing and stationary fluid [10].

Dam break flows occur when a volume of fluid is instantaneously released and flows throughout a domain, driven by gravitational forces. This type of unsteady fluid motion has been widely studied in hydraulic engineering and has wide-ranging application. For example, many large-scale, hazardous flows in the environment are generated by the rapid mobilisation of a volume of fluid and considerable insight to their motion can be gained by studying an idealised scenario in which a body of fluid, at rest within a region, is set into motion by the instantaneous removal of the boundaries that contain it. Dam break flows of this nature have a long history of published research [11–13]. They may be analysed using shallow layer theory, since the velocity is predominantly horizontal and the pressure approximately hydrostatic, are readily generated in the laboratory by removing a lock gate and releasing fluid into a flume and form a simple, yet testing, scenario for numerical simulations to reproduce.

In this paper we analyse dam break flows of fluids that exhibit yield stresses. Thus for flows over horizontal surfaces or down slopes the motion is eventually arrested because the gravitational forces driving the flow are unable to overcome the fluid's yield stress. Hence a deposit is laid down and this behaviour is in contrast with the motion in the absence of a yield stress, for which the fluid decelerates but is never arrested.

* Corresponding author.
E-mail addresses: g.matson@bristol.ac.uk (G.P. Matson), a.j.hogg@bristol.ac.uk (A.J. Hogg).

0377-0257/$ – see front matter © 2006 Elsevier B.V. All rights reserved.
doi:10.1016/j.jnnfm.2006.05.003

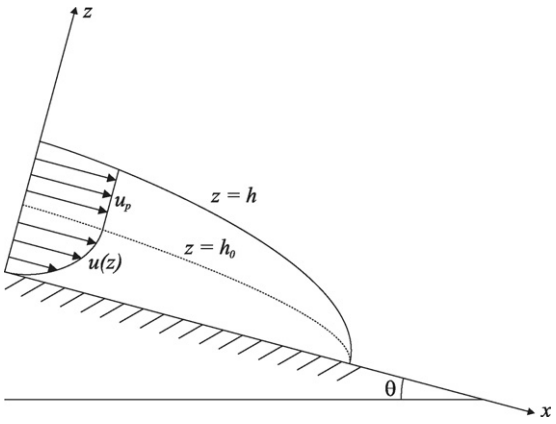

Fig. 1. Sketch of a yield stress flow showing the plug region.

Although idealised, this type of dam break flow does have some direct applications in chemical engineering and industrial processing in which the spreading of fluids needs to be precisely controlled in order to achieve the required goal. Invariably the fluids used are non-Newtonian [14] and the rheology unknown. Examples include concentrated suspensions such as concrete, pastes, foodstuffs, emulsions, foams and composites [15]. It has been suggested that careful measurements of a spreading fluid and its deposit in a 'slump test' could be used to measure rheological constants of a fluid [3]. Such a test has been used for a long time to measure the consistency of fresh concrete [16,17]. In such a test, a finite volume of fluid is instantaneously released and the final deposit used to infer the yield stress of the fluid. This is important because if the suspension is too 'stiff' it will not be possible to flow it into tight locations of mouldings. However, if it is too 'runny', the strength when hardened is reduced. In the processing of food stuffs a device called a 'Bostwick Consistometer' is used in which one measure the distance the fluid has slumped in a particular time interval to infer fluid properties [18,19]. It is important when carrying out all these tests to know when the fluid has ceased flowing and the goal of this paper is to investigate how the static fluid profile is approached.

In a geophysical context there are many complicating factors to deal with. For example, the thermal structure of lava and the particulate composition of mud will be important in defining the rheology. We ignore all such complicating factors and discuss the flow of an isothermal, viscoplastic fluid and we assume that the fluid layer is shallow and slowly moving to allow us to apply a lubrication style asymptotic reduction of the governing equations. This approach is standard practice when modelling flows of this type for both Newtonian and non-Newtonian fluids.

The paper is organised as follows. First in Section 2 we formulate the mathematical model that is employed to examine dambreak flows of viscoplastic fluids and we identify a 'lubrication' regime in which the lengthscale of the streamwise motion far exceeds the depth of the flow. This simplification yields a relatively straightforward description of the motion. Flows of fluids with yield stresses may be arrested and adopt a static profile and this is investigated in Section 3. In Section 4 we analyse the evolution of the flow towards the arrested, final state by integrating the governing equations numerically. These computations reveals that the final state is asymptotically reached and in Section 5 we investigate the approach to the arrested state analytically to explain this observation. Finally we summarise our findings and draw some brief conclusions in Section 6.

2. Mathematical formulation

We consider the two-dimensional slow flow of a sheet of incompressible, viscoplastic fluid down a plane inclined at an angle θ to the horizontal, as shown in Fig. 1. We orientate our (x', z')-coordinate system such that the x'-axis is aligned down the plane and the z'-axis is perpendicular to the plane, which is located at $z' = 0$. We denote the fluid velocity field by (u', w'), the depth of the flowing layer by $h'(x', t')$ while the fluid density and the gravitational acceleration are given by ρ and g, respectively.

We represent the rheology of the viscoplastic fluid by the Herschel–Bulkley constitutive law [4,9,20] which relates the components of the stresses, τ'_{ij}, to the strain rates, $\dot{\gamma}'_{ij} = \partial u'_i/\partial x'_j + \partial u'_j/\partial x'_i$ through the relations

$$\tau'_{ij} = \left(K_n \dot{\gamma}'^{n-1} + \frac{\tau_0}{\dot{\gamma}'}\right)\dot{\gamma}'_{ij}, \quad \text{for } \tau' \geq \tau_0, \tag{2.1}$$

$$\dot{\gamma}'_{ij} = 0, \quad \text{for } \tau' < \tau_0. \tag{2.2}$$

where K_n is the 'consistency', n a power law index that governs the degree of shear thinning or thickening, τ_0 the yield stress and τ' and $\dot{\gamma}'$ denote the second invariants of their respective tensors, given by

$$\tau' = \sqrt{\frac{\tau'_{ij}\tau'_{ij}}{2}} \quad \text{and} \quad \dot{\gamma}' = \sqrt{\frac{\dot{\gamma}'_{ij}\dot{\gamma}'_{ij}}{2}}.$$

We examine motion down the plane in the 'lubrication regime', for which the characteristic length scale along the bed, L, is much greater than the characteristic fluid depth, H. Upon defining the aspect ratio $\epsilon = H/L$, we introduce the following dimensionless variables [10]

$$\{x', z', h', t', u', w', p'\} = \left\{Lx, Hz, Hh, \frac{L}{U}t, Uu, \epsilon Uw, \rho g H \cos\theta p\right\},$$

where U denotes a downslope velocity scale, which is to be identified below, and the unadorned variables are dimensionless. Under this rescaling, the residual dimensionless parameters are the Reynolds number $Re = \rho UL/\mu$, where $\mu = K_n(U/H)^{n-1}$ is the effective viscosity for a Herschel–Bulkley fluid, the inclination of the plane θ and the Bingham number, B, given by

$$B = \frac{\tau_0}{\epsilon\rho g H \cos\theta}. \tag{2.3}$$

This parameter measures the yield stress relative to stresses generated by the weight of the flowing layer. As will be demonstrated below, its magnitude crucially determines the runout of the dam break flows and the rate at which they approach the arrested state.

We now formulate the equations governing the motion of the flowing layer in the regime of low aspect ratio ($\epsilon \ll 1$) with Reynolds number of order unity at most. Mass conservation for the flowing layer is given by

$$\frac{\partial h}{\partial t} = -\frac{\partial q}{\partial x}, \tag{2.4}$$

where q is the volume flux per unit width carried by the flow. Identifying the distinguished scaling for the downslope velocity as a balance between the pressure gradient and the divergence of the shear stresses yields $U = (\rho g H^3/\mu L)\cos\theta$ and thus the following leading order expressions for the momentum within the layer

$$0 = -\frac{\partial p}{\partial x} + S + \frac{\partial \tau_{xz}}{\partial z}, \tag{2.5}$$

$$0 = -\frac{\partial p}{\partial z} - 1, \tag{2.6}$$

where $S = \tan\theta/\epsilon$ [5,10].

Eq. (2.6) expresses hydrostatic pressure balance which can simply be integrated with the boundary condition that $p = 0$ on the free surface (using atmospheric pressure as the reference pressure) to yield

$$p(x, z, t) = h - z. \tag{2.7}$$

Upon integrating (2.5) with the stress-free boundary condition at the surface and substitution for $p(x, z, t)$ from (2.7) we obtain

$$\tau_{xz}(x, z) = \left(S - \frac{\partial h}{\partial x}\right)(h - z). \tag{2.8}$$

In order for the fluid to move, the second invariant of the stress tensor must exceed the yield stress. Thus to leading order the shear stress at the base must exceed the yield stress which in these variables means that $\tau_b = \tau_{xz}(x, 0) > B$,

$$S - \frac{\partial h}{\partial x} > \frac{B}{h}. \tag{2.9}$$

Within a flow the magnitude of the shear stress decreases linearly from τ_b at the base to zero at the free surface. If the fluid is in motion, i.e. (2.9) is satisfied, there must be some critical height, $h_0 < h$, at which the stress is equal to the yield stress generating a yield surface below which there is shearing due to the applied stress. Above this surface there is no deformation to leading order and so the flow can be considered to be plug flow.[1] By using $\tau_{xz}(x, h_0) = B$ we find

$$h_0 = h - \frac{B}{S - \partial h/\partial x}. \tag{2.10}$$

[1] This is not strictly correct as the fluid above the yield surface is not truly rigid so should be considered to be a "pseudo-plug" and the yield surface a "fake" yield surface [10].

We may now calculate the velocity profile since in the yielding region ($z < h_0$) $\tau_{xz} = B + (\partial u/\partial z)^n$, while in the plug region ($h_0 < z < h$), $\partial u/\partial z = 0$. Thus integrating (2.5), applying the no-slip boundary condition $u(0) = 0$ and ensuring that the velocity and its gradient are continuous gives

$$u(z) = \begin{cases} \frac{n}{1+n}\left(S - \frac{\partial h}{\partial x}\right)^{1/n} [h_0^{1+1/n} - (h_0 - z)^{1+1/n}], & 0 < z < h_0, \\ \frac{n}{1+n}\left(S - \frac{\partial h}{\partial x}\right)^{1/n} h_0^{1+1/n}, & h_0 < z < h. \end{cases} \tag{2.11}$$

The volume flux per unit width can be found by integrating the velocity profile over the total fluid depth, from $z = 0$ to $z = h$,

$$q = \frac{n}{1+n}\left(S - \frac{\partial h}{\partial x}\right)^{1/n} h_0^{1+1/n}\left[h - \frac{n}{1+2n}h_0\right]. \tag{2.12}$$

Combining Eq. (2.12) with (2.4) and eliminating h_0 using (2.10) we arrive at a single evolution equation for the fluid depth $h(x, t)$:

$$\frac{\partial h}{\partial t} = -\frac{n}{1+2n}\frac{\partial}{\partial x}\left[\left(S - \frac{\partial h}{\partial x}\right)^{-2}\left(h\left(S - \frac{\partial h}{\partial x}\right) - B\right)^{1+1/n}\left(h\left(S - \frac{\partial h}{\partial x}\right) + \frac{n}{1+n}B\right)\right], \tag{2.13}$$

under the condition given by (2.9) [5,14].

In what follows, we restrict our analysis to the simpler case of dam break flows over a horizontal surface ($S = 0$), noting that the techniques presented below and analogous results may be derived when $S > 0$. Therefore, for this study, our governing equation is given by

$$\frac{\partial h}{\partial t} = \frac{n}{1+2n}\frac{\partial}{\partial x}\left[\left(\frac{\partial h}{\partial x}\right)^{-2}\left(-h\frac{\partial h}{\partial x} - B\right)^{1+1/n}\left(h\frac{\partial h}{\partial x} - \frac{n}{1+n}B\right)\right], \tag{2.14}$$

under the condition that the yield stress is exceeded and the fluid flows, which is given by

$$-h\frac{\partial h}{\partial x} > B. \tag{2.15}$$

3. Dam break flows on a horizontal plane

We now analyse the motion that arises when fluid is instantaneously released from behind a lockgate and flows over an initially dry, horizontal bed. An impenetrable back wall of the lock is located at $x = 0$ and the lockgate is at $x = 1$. The depth of the fluid initially within the lock is unity and thus the initial condition for the dam break flow is

$$h(x) = \begin{cases} 1, & 0 \le x \le 1, \\ 0, & x > 1. \end{cases} \tag{3.1}$$

The fluid intrudes forward over the horizontal bed and its front is at position $x = x_f(t)$ where $h(x_f, t) = 0$ for all time. The volume of fluid is conserved throughout the flow and thus

$$\int_0^{x_f} h\,\mathrm{d}x = 1. \tag{3.2}$$

Initially the yield criterion (2.15) will be exceeded at the front of the flow causing the fluid to flow, but as time evolves the fluid will reach a static profile, $h_\infty(x)$, at which the yield criterion is not exceeded anywhere. If the Bingham number, B, is sufficiently large, there will exist a point which we term the yield point, $x_{y\infty}$, behind which the fluid does not flow during any of the motion (see Fig. 2(a)). If however the Bingham number is sufficiently small, then all of the fluid will flow and the yield point will not exist (see Fig. 2(b)). In the region of fluid flow, motion is arrested when the yield condition, (2.15), becomes an equality and for motion over a horizontal surface, the profile will be of the form of

$$h^2 - h_*^2 = -2B(x - x_*), \tag{3.3}$$

where the integration constant is chosen so that $h = h_*$ at $x = x_*$.

If we assume that a yield point exists then we must force the profile to have height equal to unity at $x_{y\infty}$. Thus the arrested profile is given by

$$h_\infty(x) = \begin{cases} 1, & 0 \le x \le x_{y\infty}, \\ \sqrt{1 + 2B(x_{y\infty} - x)}, & x_{y\infty} < x \le x_{f\infty}. \end{cases} \tag{3.4}$$

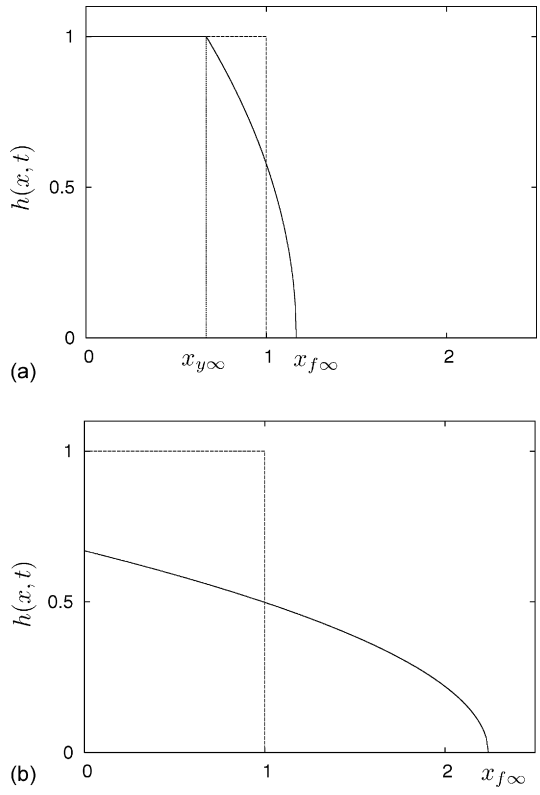

Fig. 2. The initial profile of fluid (dashed line) and two examples of final deposits (solid lines). If $B > 1/3$ not all of the fluid takes part in the motion and there is a discontinuity in the gradient of the final height profile as shown in example (a), for which $B = 1$. However, if $B < 1/3$ all of the fluid flows and the final profile will be of the form (b), for which $B = 0.1$.

Also we have that at the front of the flow the height must vanish yielding a relationship between $x_{\mathrm{f}\infty}$ and $x_{\mathrm{y}\infty}$,

$$x_{\mathrm{f}\infty} = x_{\mathrm{y}\infty} + \frac{1}{2B}. \tag{3.5}$$

The point $x_{\mathrm{y}\infty}$, and hence $x_{\mathrm{f}\infty}$, can now be found by enforcing conservation of volume,

$$\int_0^{x_{\mathrm{f}\infty}} h_\infty(x)\,\mathrm{d}x = 1, \tag{3.6}$$

and we obtain

$$x_{\mathrm{y}\infty} = 1 - \frac{1}{3B} \qquad \text{and} \qquad x_{\mathrm{f}\infty} = 1 + \frac{1}{6B}. \tag{3.7}$$

The above analysis is only valid if the yield point does not reach the back wall, $x_{\mathrm{y}\infty} > 0$, therefore only if $B > 1/3$. The intermediate value, $B = 1/3$, corresponds to the case for which the yield point is exactly at the origin and for B below this value a different approach is required. In this latter regime the profile will still be in the form of (3.3) but we must this time force the height at the front to be zero,

$$h_\infty(x) = \sqrt{2B(x_{\mathrm{f}\infty} - x)}. \tag{3.8}$$

By enforcing volume conservation again we obtain

$$x_{\mathrm{f}\infty} = \left(\frac{9}{8B}\right)^{1/3}. \tag{3.9}$$

In summary the static profile deposits will be of the form:

$$B \geq \frac{1}{3} \qquad x_{\mathrm{f}\infty} = 1 + \frac{1}{6B}, \qquad x_{\mathrm{y}\infty} = 1 - \frac{1}{3B}, \tag{3.10}$$

$$h_\infty(x) = \begin{cases} 1, & 0 \leq x \leq x_{\mathrm{y}\infty}, \\ \sqrt{\frac{1}{3} + 2B(1-x)}, & x_{\mathrm{y}\infty} < x \leq x_{\mathrm{f}\infty}, \end{cases} \tag{3.11}$$

$$B < \frac{1}{3} \qquad x_{f\infty} = \left(\frac{9}{8B}\right)^{1/3}, \tag{3.12}$$

$$h_\infty(x) = \sqrt{2B\left[\left(\frac{9}{8B}\right)^{1/3} - x\right]}. \tag{3.13}$$

As is expected from the nature of the system, $x_{f\infty}$ and $h_\infty(x)$ vary continuously from one regime to the other. The static profile for $B = 1$ is plotted in Fig. 2(a) and for $B = 0.1$ in Fig. 2(b).

4. Flow evolution

The dam break flow of a fluid without a yield stress ($B = 0$) has been well studied. For a viscous, Newtonian fluid ($n = 1$), see Didden and Maxworthy [21] and Huppert [7] while power-law fluids were studied by Gratton and Minotti [22]. In the absence of a yield stress ($B = 0$), the dam break flow cannot be arrested. The governing equation, (2.14), reduces to

$$\frac{\partial h}{\partial t} = \frac{n}{1+2n}\frac{\partial}{\partial x}\left(h^{2+1/n}\left|\frac{\partial h}{\partial x}\right|^{1/n-1}\frac{\partial h}{\partial x}\right). \tag{4.1}$$

For a Newtonian fluid ($n = 1$) this governing partial differential equation has been extensively researched. Huppert [7] showed that the long time behaviour is governed by a similarity solution which is the intermediate asymptotic for the solutions from sufficiently regular initial conditions and that laboratory realisations of the flows rapidly adjust to states that are well represented by this solution. More recently Gratton and Minotti [22] have derived similarity solutions for more general power-law fluids,

$$h(x,t) = K^{(n+1)/(n+2)}t^{-n/(2n+3)}\left(\frac{2n+1}{2n+3}\right)^{n/(n+2)}\left(\frac{n+2}{n+1}\right)^{1/(n+2)}\left[1-\left(\frac{x}{Kt^{n/(2n+3)}}\right)^{n+1}\right]^{1/(n+2)}, \tag{4.2}$$

where K satisfies the relation

$$K^{2n+3} = \frac{(n+1)^{n+3}}{n+2}\left(\frac{2n+3}{2n+1}\right)^{n}\left[\beta\left(\frac{1}{n+1},\frac{n+3}{n+2}\right)\right]^{-n-2}, \tag{4.3}$$

and $\beta(r, s)$ is a beta-function. Thus, the position of the front is at $Kt^{n/(2n+3)}$.

The added complexity of incorporating a yield stress make this analytical route impossible and so below we detail a numerical scheme to solve (2.14). However, the existence of the analytical solution above provides us with a useful tool to check the numerical schemes accuracy in certain circumstances.

4.1. Numerical scheme

In order to solve (2.14) we integrate it using an explicit finite difference scheme which is second order in both time and space. Before differencing the equations we make a change of variable,

$$\xi = \frac{x - x_y}{x_f - x_y}, \tag{4.4}$$

where $x_f(t)$ and $x_y(t)$ are the instantaneous positions of the front of the flow and the yield point, respectively. For $x = x_f$ we have $h = 0$ so may readily enforce the boundary condition $h(\xi = 1, t) = 0$ for all t. For $0 \le x \le x_y$ we have $h(x) = 1$ and may enforce the boundary condition $h(\xi = 0, t) = 1$. If, however, $x_y = 0$ we must apply the no flux condition at the back wall, given by (2.15) as an equality,

$$\left.\frac{\partial}{\partial\xi}h^2\right|_{\xi=0} = -2Bx_f. \tag{4.5}$$

The active section of the profile, within which (2.15) is satisfied, thus corresponds to the fixed domain $0 \le \xi \le 1$. To simplify notation we introduce the active length, $x_a(t) = x_f(t) - x_y(t)$, and thus treating ξ and t as the independent variables, the governing Eq. (2.14) becomes

$$\frac{\partial h}{\partial t} - \frac{1}{x_a}\left(\xi\dot{x}_a + \dot{x}_y\right)\frac{\partial h}{\partial\xi} = \frac{n}{1+2n}x_a\frac{\partial}{\partial\xi}\left[\left(\frac{\partial h}{\partial\xi}\right)^{-2}\left(-\frac{h}{x_a}\frac{\partial h}{\partial\xi} - B\right)^{1+1/n}\left(\frac{h}{x_a}\frac{\partial h}{\partial\xi} - \frac{n}{1+n}B\right)\right], \tag{4.6}$$

where a dot denotes differentiation with respect to time. This equation is applied only in the region $0 < \xi < 1$.

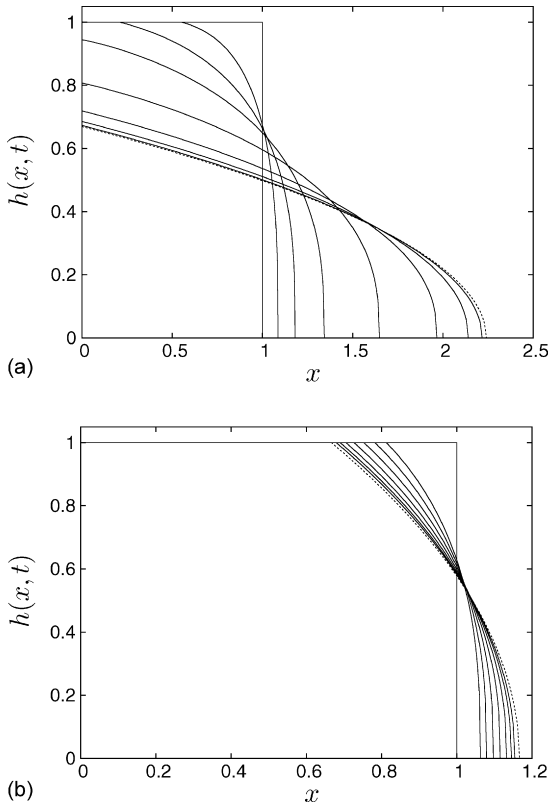

Fig. 3. Snapshots of the fluid profile, $h(x, t)$ at various times for (a) $B = 0.1$ and (b) $B = 1$. The dashed lines show the final profile.

In order to obtain a full solution the points x_y and x_a must both be tracked. In order to track x_y we initially assume $x_y > 0$ and apply Eq. (4.6) at $\xi = 0$ using $h = 1$ and $\partial h/\partial t = 0$ to obtain[2]

$$\dot{x}_y = -\frac{n}{1+2n} x_a^2 \left(\frac{\partial h}{\partial \xi}\bigg|_{\xi=0} \right)^{-1} \frac{\partial}{\partial \xi} \left[\left(\frac{\partial h}{\partial \xi} \right)^{-2} \left(-\frac{1}{x_a} \frac{\partial h}{\partial \xi} - B \right)^{1+1/n} \left(\frac{1}{x_a} \frac{\partial h}{\partial \xi} - \frac{n}{1+n} B \right) \right]_{\xi=0}. \tag{4.7}$$

Using (4.7) we can propagate x_y back from its initial value close to one. If at any point x_y becomes less than zero it means the flow has reached the back wall and we can hence no longer apply $h = 1$. In this case we then fix $x_y = 0$ and apply condition (4.5) to find the gradient of the profile at the back wall. In order to evolve x_a, and hence x_f, we use mass conservation, (3.2), in the new coordinate system with the already calculated value of x_y,

$$\int_0^1 h(\xi, t)\, \mathrm{d}\xi = \frac{1 - x_y}{x_a}. \tag{4.8}$$

We use an explicit finite difference scheme to solve the governing equation in the case of a Bingham fluid ($n = 1$), details of which are given in Appendix A. The numerical code was validated by comparison with the known similarity solution for a Newtonian fluid [7] in which the numerical and analytical profiles were indistinguishable. In addition for cases with nonzero B the numerically computed and predicted end states (see (3.10)–(3.13)) compare favourably. Resolution testing was carried out and it is found that in order to maintain stability of the profile we required $\delta t \sim \delta x^2 = x_a^2 \delta\xi^2$. No significant gain was found by increasing the resolution beyond $\delta\xi = 0.01$. Using this resolution on an Intel Pentium 4 2.8 GHz with 512 MB RAM the runtime for a typical dimensionless time unit was 8 s.

4.2. Flow evolution for a Bingham fluid

The numerical method described above was employed to investigate the evolution of dam break flows of viscoplastic fluids with $n = 1$. Examples with $B = 0.1$ and 1 are plotted in Fig. 3. In both cases the asymptotic profile obtained from (3.11) and (3.13) is

[2] Expanding h in the regime $\xi \ll 1$ reveals a non-trivial fractional power dependance close to the yield point ($\xi = 0$), $h(\xi) = 1 - Bx_a\xi + \chi\xi^{(2n+1)/(n+1)} + \cdots$, where χ is a constant.

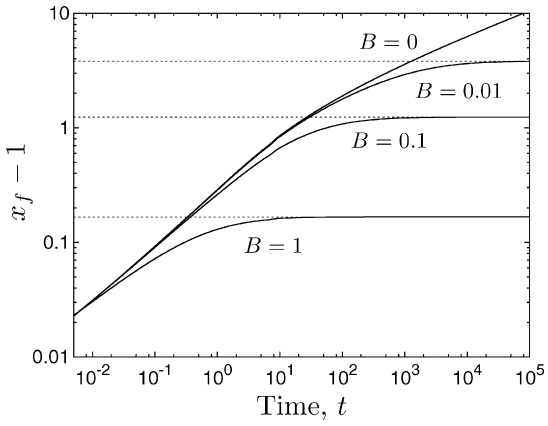

Fig. 4. The position of the front, x_f, as a function of time. The horizontal dashed lines show the expected final values.

also plotted. In Fig. 4 the front position is plotted for various Bingham numbers. It can be seen that for $B = 1$ the front position very quickly approaches a limiting value but for lower values of B it continues to increase for longer. Also we see that increasing the Bingham number causes the fluid to propagate slower as would be expected.

5. Approach to final state

The numerical simulations show that the dam break flows evolve towards the steady-state in which the fluid is arrested and at the point of yielding. However, the adjustment towards this final state is long and hence it is of considerable interest to elucidate the approach to the arrested state in the regime $t \gg 1$. Indeed this may have important practical consequences since in an experiment or rheological test one may wish to assess when the fluid has finally arrested.

5.1. Low yield stress: $B < 1/3$

We first consider cases with $B < 1/3$ in which the yield point reaches the back wall before the motion arrests. For large time it is therefore sufficient to assume that $x_y = 0$ and hence $x_a = x_f$. By considering the height profile as a function of ξ it can be seen that $h(\xi, t)$ must always be greater then the asymptotic profile, $h_\infty(\xi)$, and that the front position, $x_f(t)$ must always be less than $x_{f\infty}$. Thus we define the positive perturbation variables, $\tilde{h}(\xi, t)$ and $\tilde{x}_f(t)$, to these arrested states

$$h(\xi, t) = h_\infty(\xi) + \tilde{h}(\xi, t), \tag{5.1}$$

$$x_f(t) = x_{f\infty} - \tilde{x}_f(t), \tag{5.2}$$

where we assume that $\tilde{h}/h_\infty \ll 1$ and $\tilde{x}_f/x_{f\infty} \ll 1$ and $x_{f\infty}$ and $h_\infty(\xi)$ are given by (3.12) and (3.13). On substituting (5.1) and (5.2) into the governing Eq. (4.6) we can make a series expansion in these perturbation variables. Using our knowledge of the asymptotic state from setting condition (2.15) to an equality,

$$-\frac{h_\infty}{x_{f\infty}}\frac{\partial h_\infty}{\partial \xi} = B, \tag{5.3}$$

it may be observed that the leading order terms in the perturbation variables on the right-hand side of (4.6) have exponent $1 + 1/n$, whereas those on the left-hand side are of exponent 1. Upon carrying out the expansion and using (5.3) we obtain

$$\frac{\partial \tilde{h}}{\partial t} - \frac{\xi B}{h_\infty}\frac{\mathrm{d}\tilde{x}_f}{\mathrm{d}t} = -\frac{n}{1+n}\frac{B^{1/n}}{x_{f\infty}}\frac{\partial}{\partial \xi}\left[h_\infty^2\left(\frac{\tilde{h}}{h_\infty} + \frac{\tilde{x}_f}{x_{f\infty}} - \frac{h_\infty}{B x_{f\infty}}\frac{\partial \tilde{h}}{\partial \xi}\right)^{1+1/n}\right]. \tag{5.4}$$

The first order expression of mass conservation, (3.2), yields

$$\int_0^1 \tilde{h}\,\mathrm{d}\xi = \frac{\tilde{x}_f}{x_{f\infty}^2}, \tag{5.5}$$

and the no flux condition at $\xi = 0$, (4.5), to first order becomes

$$\left.\frac{\partial \tilde{h}}{\partial \xi}\right|_{\xi=0} - \frac{1}{2}\tilde{h}(\xi = 0) = \left(\frac{B^2}{3}\right)^{1/3}\tilde{x}_f, \tag{5.6}$$

having used the profile of the final state from (3.13) which in these variables reduces to $h_\infty(\xi) = (3B)^{1/3}\sqrt{1-\xi}$.

To solve for the first order perturbations, we construct a solution in separable form, $\tilde{h}(\xi, t) = A(\xi)G(t)$ and $\tilde{x}_f(t) = F(t)$, where both $F, G \to 0$ as $t \to \infty$. Upon substitution into (5.5) it is found that $G(t)$ is simply a constant multiple of $F(t)$, so it is possible to absorb this constant into the definition of $A(\xi)$. Upon substitution of the known final profile from (3.12) and (3.13) it is also useful to write $A(\xi) = (B^2/3)^{1/3}E(\xi)$ and thus we seek solutions of the form

$$\tilde{h}(\xi, t) = \left(\frac{B^2}{3}\right)^{1/3} E(\xi)F(t), \tag{5.7}$$

$$\tilde{x}_f(t) = F(t). \tag{5.8}$$

Substitution of these into (5.4) and separation of terms yields

$$\frac{1}{F^{1+1/n}}\frac{dF}{dt} = -\frac{2n}{1+n}\left(\frac{B^2}{3}\right)^{(2+n)/(3n)} \frac{(d/d\xi)[(1-\xi)\{(1-\xi)^{-1/2}E + 2 - 2(1-\xi)^{1/2}(dE/d\xi)\}^{1+1/n}]}{E - \xi(1-\xi)^{-1/2}}. \tag{5.9}$$

The left hand side of (5.9) is solely a function of time and the right hand side solely a function of ξ so they must both be equal to a constant. For notational convenience we chose the constant

$$k = \frac{E - \xi(1-\xi)^{-1/2}}{(d/d\xi)[(1-\xi)\{(1-\xi)^{-1/2}E + 2 - 2(1-\xi)^{1/2}(dE/d\xi)\}^{1+1/n}]}, \tag{5.10}$$

and we obtain an ODE for $F(t)$,

$$\frac{1}{F^{1+1/n}}\frac{dF}{dt} = -\frac{2n}{1+n}\left(\frac{B^2}{3}\right)^{(2+n)/(3n)} \frac{1}{k}. \tag{5.11}$$

Integration of this equation leads us to the solution

$$F(t) = \left[\frac{1+n}{2}\left(\frac{3}{B^2}\right)^{(2+n)/(3n)} \frac{k}{t}\right]^n, \tag{5.12}$$

where the constant of integration has been set to zero. This is appropriate because the constant sets the origin of time, but we are only interested in large time so we may choose it arbitrarily.

In order to complete the solution we need to solve the spatial ODE given by (5.10) to determine k. We make the following changes of independent and dependant variables,

$$\tau = \sqrt{1-\xi}, \qquad E(\xi) = \frac{1 - P(\tau)}{\tau} - \tau, \tag{5.13}$$

and find that the equation reduces to

$$P = \frac{k}{2}\frac{d}{d\tau}\left[\tau^2\left(-\frac{1}{\tau}\frac{dP}{d\tau}\right)^{1+1/n}\right]. \tag{5.14}$$

The perturbation must vanish at the front of the flow for all time, therefore we must have $E(\xi = 1) = 0 \Rightarrow P(\tau = 0) = 1$. Analysing (5.10) indicates that this is a regular singular point of the equation and therefore by making an expansion close to $\tau = 0$ we can obtain the value of P and its derivative here. Making the substitution $P(\tau) = 1 + C\tau^\alpha$, where α is a constant to be found, and taking a dominant term balance for $\tau \ll 1$ we obtain

$$P(\tau) \sim 1 - \frac{1+n}{2+n}\left(\frac{2}{k}\right)^{n/(1+n)} \tau^{(2+n)/(1+n)} \qquad \textit{for } \tau \ll 1 \tag{5.15}$$

This provides us with two conditions at $\tau = 0$ but in order to determine k we need one further condition and this is obtained from mass conservation, (5.5), which upon substitution of the separable solution yields

$$\int_0^1 E(\xi)\,d\xi = \frac{4}{3} \qquad \Rightarrow \qquad \int_0^1 P(\tau)\,d\tau = 0. \tag{5.16}$$

Equivalently we could use the condition at the back wall, (5.6), which yields

$$\left.\frac{dE}{d\xi}\right|_{\xi=0} - \frac{E(\xi = 0)}{2} = 1 \qquad \Rightarrow \qquad \left.\frac{dP}{d\tau}\right|_{\tau=1} = 0. \tag{5.17}$$

The system may now be simply integrated numerically by initiating a solution with $\tau \ll 1$ using (5.15), integrating to $\tau = 1$ and adjusting k such that the boundary conditions (5.16) and (5.17) are satisfied. Results for various n are displayed in Fig. 5 and the corresponding values of k in Table 1.

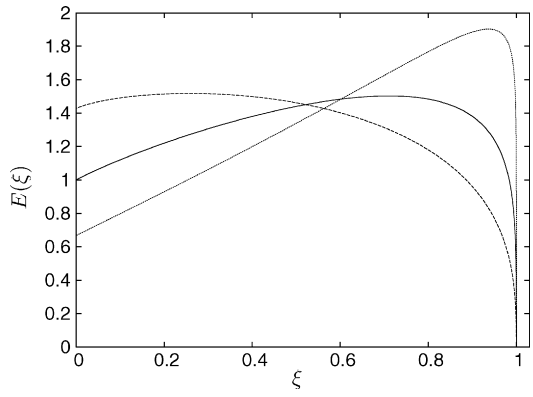

Fig. 5. The spatial perturbation $E(\xi)$ as a function of the re-scaled distance, ξ, when $B < 1/3$ for different power law indices, $n = 1$ (solid line), 1/3 (−−) ,3 (· · ·).

Table 1
Values of the constants k and λ for different power law indices

n	k	λ
1/5	0.3758	1.5992
1/3	0.2936	1.4280
1/2	0.2159	1.2724
1	0.08663	1.0000
2	0.01419	0.7693
3	0.002345	0.6669
5	0.00006460	0.5721

See (5.10) and (5.37) for the definitions.

In summary, the perturbation variables decrease as $1/t^n$ for $t \gg 1$,

$$\tilde{x}_f(t) = \left[\frac{(1+n)k}{2}\right]^n \left(\frac{3}{B^2}\right)^{(2+n)/3} \frac{1}{t^n}, \tag{5.18}$$

$$\tilde{h}(\xi, t) = \left[\frac{(1+n)k}{2}\right]^n \left(\frac{3}{B^2}\right)^{(1+n)/3} \frac{E(\xi)}{t^n}. \tag{5.19}$$

An application of the above theory is to determine how long it takes for the length of a flow to reach a proportion, $(1-\delta)$, of its final length, $x_{f\infty}$, where we assume $\delta \ll 1$ to ensure we are within the regime of validity of the above perturbation analysis. At this time, $t_s(\delta)$, we have $\tilde{x}_f = \delta x_{f\infty}$ which, upon using (5.18), can be solved to find

$$t_s(\delta) = \frac{(1+n)k}{2} \left(\frac{2}{\delta}\right)^{1/n} \frac{3^{1/3}}{B^{(2n+3)/3n}}. \tag{5.20}$$

This prediction could be used in industrial tests in which it is assumed the fluid has arrested its motion. As has been shown, motion is not arrested in a finite time, but (5.20) provides the time taken for the slump to attain a distance $(1-\delta)x_{f\infty}$.

5.1.1. Bingham fluid ($n = 1$)

In the special case of a Bingham fluid, in which $n = 1$, (5.14) reduces to

$$P = k\frac{\mathrm{d}P}{\mathrm{d}\tau}\frac{\mathrm{d}^2P}{\mathrm{d}\tau^2} = kP'^2\frac{\mathrm{d}P'}{\mathrm{d}P}, \tag{5.21}$$

where $P' = \mathrm{d}P/\mathrm{d}\tau$, and this can be integrated analytically. A first integration and application of the behaviour at $\tau = 0$ from (5.15) yields

$$\frac{\mathrm{d}P}{\mathrm{d}\tau} = \left(\frac{3}{2k}\right)^{1/3} (P^2-1)^{1/3}. \tag{5.22}$$

Subsequent integration yields the solution in implicit form,

$$\left(\frac{3}{2k}\right)^{1/3} \tau = \int_1^P \frac{\mathrm{d}\hat{P}}{(\hat{P}^2-1)^{1/3}}. \tag{5.23}$$

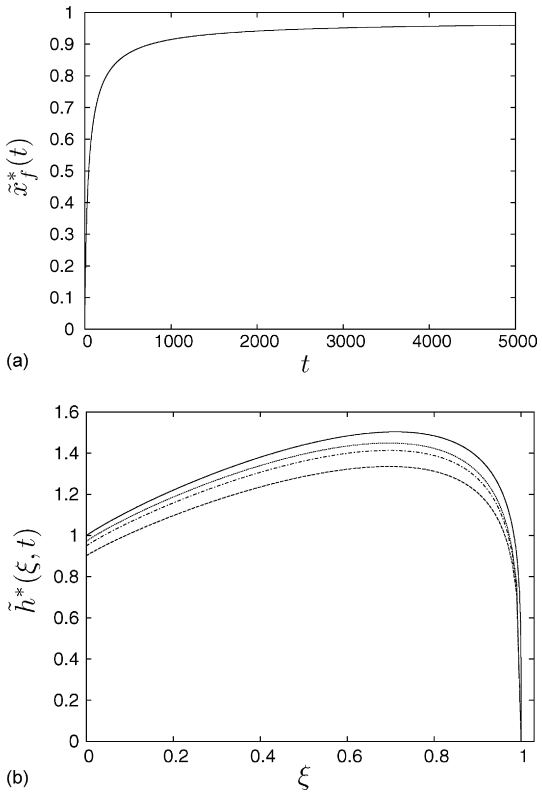

Fig. 6. Numerical results for $B = 0.1$. (a) The scaled front position, x_f^*, as a function of time; (b) The rescaled spatial perturbation approaching the analytical solution of $E(\xi)$ (solid line) for dimensionless times $t = 500$ (– –), 1500 (·–), 5000 (· · ·).

This integral can be written in terms of the hypogeometric function ${}_2F_1(\frac{1}{3}, \frac{1}{2}; \frac{3}{2}; P^2)$ and $P(\tau)$ written implicitly as

$$\left(\frac{3}{2k}\right)^{1/3} \tau = \left[-\hat{P}_2 \; F_1\left(\frac{1}{3}, \frac{1}{2}; \frac{3}{2}; \hat{P}^2\right)\right]_1^P. \tag{5.24}$$

Combining (5.22) with the boundary condition at $\tau = 1$ from (5.17) it is possible to deduce that $P(\tau = 1) = \pm 1$. The initial spatial perturbation, $\tilde{h}$ must be positive which implies that $E(\xi) > 0$ for all ξ which in turn implies that the correct sign is negative, $P(\tau = 1) = -1$. Applying this to (5.23) gives an analytical solution for k in terms of gamma functions,

$$k = \frac{1}{18}\left(\frac{\sqrt{\pi}}{\Gamma(2/3)\Gamma(5/6)}\right)^3 = 0.0866257. \tag{5.25}$$

Using this value for k and plotting (5.24), we find that the solution agrees exactly with that found numerically for $n = 1$.

5.1.2. Comparison with numerical results

We now compare this asymptotic analysis with the numerical results for the case $n = 1$. To this end we construct the rescaled parameters

$$\tilde{x}_\mathrm{f}^*(t) = \frac{1}{k}\frac{B^2}{3} t\tilde{x}_\mathrm{f}(t), \tag{5.26}$$

$$\tilde{h}^*(\xi, t) = \frac{1}{k}\left(\frac{B^2}{3}\right)^{2/3} t\,\tilde{h}(\xi, t). \tag{5.27}$$

where we anticipate that $\tilde{x}_\mathrm{f}^*(t) \to 1$ and $\tilde{h}^*(\xi, t) \to E(\xi)$ in the limit $t \to \infty$. Fig. 6 shows $\tilde{x}_\mathrm{f}^*$ and $\tilde{h}^*$ plotted as a function of time for $B = 0.1$. It is readily observed that the numerics do rapidly approach these asymptotic states, confirming our analysis.

5.2. High yield stress: $B > 1/3$

The case of $B \geq 1/3$ is slightly more complicated than that already considered because with the addition of the yield point, x_y, there are three variables approaching their asymptotic value. We notice that $x_\mathrm{y}(t)$ must always be greater than $x_{\mathrm{y}\infty}$ and hence define

the positive perturbation variables, $\tilde{h}(\xi, t)$, $\tilde{x}_{\mathrm{f}}(t)$ and $\tilde{x}_{\mathrm{y}}(t)$, to the arrested states

$$h(\xi, t) = h_{\infty}(\xi) + \tilde{h}(\xi, t), \tag{5.28}$$

$$x_{\mathrm{f}}(t) = x_{\mathrm{f}\infty} - \tilde{x}_{\mathrm{f}}(t), \tag{5.29}$$

$$x_{\mathrm{y}}(t) = x_{\mathrm{y}\infty} + \tilde{x}_{\mathrm{y}}(t), \tag{5.30}$$

where we assume that $\tilde{h}/h_{\infty} \ll 1$, $\tilde{x}_{\mathrm{f}}/x_{\mathrm{f}\infty} \ll 1$ and $\tilde{x}_{\mathrm{y}}/x_{\mathrm{y}\infty} \ll 1$ and $x_{\mathrm{f}\infty}, x_{\mathrm{y}\infty}$ and $h_{\infty}(\xi)$ are given by (3.7) and (3.11). On substituting (5.28)–(5.30) into the governing Eq. (4.6) and using the asymptotic condition from (2.15) as an equality,

$$-\frac{h_{\infty}}{x_{\mathrm{f}\infty} - x_{\mathrm{y}\infty}} \frac{\partial h_{\infty}}{\partial \xi} = B, \tag{5.31}$$

we can make a series expansion in these perturbation variables to yield

$$\frac{\partial \tilde{h}}{\partial t} - \frac{B}{h_{\infty}} \left[\xi \left(\frac{\mathrm{d}\tilde{x}_{\mathrm{f}}}{\mathrm{d}t} + \frac{\mathrm{d}\tilde{x}_{\mathrm{y}}}{\mathrm{d}t} \right) - \frac{\mathrm{d}\tilde{x}_{\mathrm{y}}}{\mathrm{d}t} \right] = -\frac{n}{1+n} \frac{B^{1/n}}{x_{\mathrm{a}\infty}} \frac{\partial}{\partial \xi} \left[h_{\infty}^2 \left(\frac{\tilde{h}}{h_{\infty}} + \frac{\tilde{x}_{\mathrm{f}} + \tilde{x}_{\mathrm{y}}}{x_{\mathrm{a}\infty}} - \frac{h_{\infty}}{B x_{\mathrm{a}\infty}} \frac{\partial \tilde{h}}{\partial \xi} \right)^{1+1/n} \right], \tag{5.32}$$

where $x_{\mathrm{a}\infty} = x_{\mathrm{f}\infty} - x_{\mathrm{y}\infty} = 1/(2B)$. The first order expression of conservation of mass, (3.2), yields

$$\int_0^1 \tilde{h} \, \mathrm{d}\xi = \frac{1 - x_{\mathrm{y}\infty}}{x_{\mathrm{a}\infty}^2} \left(\tilde{x}_{\mathrm{f}} - \tilde{x}_{\mathrm{y}} \right) - \frac{\tilde{x}_{\mathrm{y}}}{x_{\mathrm{a}\infty}}. \tag{5.33}$$

and the no flux condition at $\xi = 0$, (4.5), to first order becomes

$$\left. \frac{\partial \tilde{h}}{\partial \xi} \right|_{\xi=0} - \frac{1}{2} \tilde{h}(\xi = 0) = B(\tilde{x}_{\mathrm{f}} + \tilde{x}_{\mathrm{y}}), \tag{5.34}$$

having used the asymptotic profile state from (3.11) which in these variables reduces to $h_{\infty}(\xi) = \sqrt{1 - \xi}$. One further condition is required to fix $\tilde{x}_{\mathrm{y}}$ and this is given by the knowledge that $h(0, t) = 1$ for all time.

To solve this first order problem we construct a solution in separable form, $\tilde{h}(\xi, t) = A(\xi)G(t)$, $\tilde{x}_{\mathrm{f}}(t) = F(t)$ and $\tilde{x}_{\mathrm{y}}(t) = H(t)$, where $F, G, H \to 0$ as $t \to \infty$. Upon substitution into (5.33) and (5.34) it is found that $F(t)$ and $H(t)$ must differ only by a multiplicative constant and $G(t)$ is simply a constant multiple of some addition of $F(t)$ and $H(t)$. Upon substitution of the known final profile it is found that it is useful to write $A(\xi) = BE(\xi)$ and thus

$$\tilde{h}(\xi, t) = BE(\xi)F(t), \tag{5.35}$$

$$\tilde{x}_{\mathrm{f}}(t) = F(t), \tag{5.36}$$

$$\tilde{x}_{\mathrm{y}}(t) = \lambda F(t), \tag{5.37}$$

where λ is a constant to be found. Substitution of this into (5.30) and separation of terms yields

$$\frac{1}{F^{1+1/n}} \frac{\mathrm{d}F}{\mathrm{d}t} = -\frac{2n}{1+n} B^{(2+n)/n} \frac{(\mathrm{d}/\mathrm{d}\xi)[(1-\xi)\{(1-\xi)^{-1/2}E + 2(1+\lambda) - 2(1-\xi)^{1/2}(\mathrm{d}E/\mathrm{d}\xi)\}^{1+1/n}]}{E - (\xi - \lambda(1-\xi))(1-\xi)^{-1/2}}. \tag{5.38}$$

The left hand side of (5.38) is solely a function of time and the right hand side solely a function of ξ so they must both be equal to a constant. For notational convenience we chose the constant

$$k = \frac{E - (\xi - \lambda(1-\xi))\,(1-\xi)^{-1/2}}{(\mathrm{d}/\mathrm{d}\xi)[(1-\xi)\{(1-\xi)^{-1/2}E + 2(1+\lambda) - 2(1-\xi)^{1/2}(\mathrm{d}E/\mathrm{d}\xi)\}^{1+1/n}]}, \tag{5.39}$$

and we obtain an ODE for $F(t)$,

$$\frac{1}{F^{1+1/n}} \frac{\mathrm{d}F}{\mathrm{d}t} = -\frac{2n}{1+n} B^{(2+n)/n} \frac{1}{k}. \tag{5.40}$$

Integration of this equation leads us to the solution

$$F(t) = \left[\frac{1+n}{2} \left(\frac{1}{B} \right)^{(2+n)/n} \frac{k}{t} \right]^n, \tag{5.41}$$

where the constant of integration has been set to zero as before. If we take the limiting case, $B = 1/3$, it is seen that this solution agrees with (5.12) as expected.

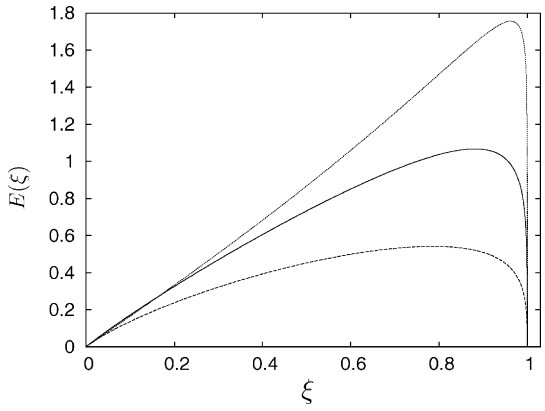

Fig. 7. The spatial perturbation $E(\xi)$, as a function of rescaled distance, ξ, when $B > 1/3$ for different power law indices, $n = 1$ (solid line), 1/3 (– –), 3 (· · ·).

In order to complete the solution we need to solve the spatial ODE given by (5.39) to determine k. We make a similar change of independent and dependent variables as before,

$$\tau = \sqrt{1-\xi}, \qquad E(\xi) = \frac{1-P(\tau)}{\tau} - (1+\lambda)\tau, \tag{5.42}$$

and the equation reduces identically to (5.14) with the same boundary conditions, (5.15)–(5.17). The one extra boundary condition given by the vanishing height at $\xi = 0$ implies that the perturbation to the height must also vanish and hence $E(\xi = 0) = 0$ which reduces to

$$P(\tau = 1) = -\lambda. \tag{5.43}$$

The solution for $P(\tau)$ is identical to that in Section 5.1 and the value of k the same as before written alongside λ in Table 1. However the conversion back to $E(\xi)$ yields different results due to the dependance on λ and this is plotted in Fig. 7.

In summary, the perturbation variables decrease as $1/t^n$ for $t \gg 1$,

$$\tilde{x}_\mathrm{f}(t) = \left[\frac{(1+n)k}{2}\right]^n \left(\frac{1}{B}\right)^{2+n} \frac{1}{t^n}, \tag{5.44}$$

$$\tilde{x}_\mathrm{y}(t) = \lambda \left[\frac{(1+n)k}{2}\right]^n \left(\frac{1}{B}\right)^{2+n} \frac{1}{t^n}, \tag{5.45}$$

$$\tilde{h}(\xi, t) = \left[\frac{(1+n)k}{2}\right]^n \left(\frac{1}{B}\right)^{1+n} \frac{E(\xi)}{t^n}. \tag{5.46}$$

As before we can proceed to find a time, $t_\mathrm{s}(\delta)$ at which the flow has reached a proportion $(1-\delta)$ of its asymptotic value. Applying $\tilde{x}_\mathrm{f} = \delta x_{\mathrm{f}\infty}$ and using (5.44), we find

$$t_\mathrm{s}(\delta) = \frac{(1+n)k}{2} \left(\frac{6}{\delta B^{1+n}(1+6B)}\right)^{1/n}. \tag{5.47}$$

5.2.1. Bingham fluid ($n = 1$), comparison with numerical results

In the special case of a Bingham fluid ($n = 1$) the equations can be solved analytically as demonstrated in Section 5.1.1 and k found to be given by (5.25) and $\lambda = 1$. In order to compare the asymptotic analysis with the numerical results we construct the rescaled parameters

$$\tilde{x}^*_\mathrm{f}(t) = \frac{B^3}{k}\, t\tilde{x}_\mathrm{f}(t), \tag{5.48}$$

$$\tilde{x}^*_\mathrm{y}(t) = \frac{B^3}{k}\, t\tilde{x}_\mathrm{y}(t), \tag{5.49}$$

$$\tilde{h}^*(\xi, t) = \frac{B^2}{k}\, t\tilde{h}(\xi, t)\,. \tag{5.50}$$

where we anticipate $\tilde{x}^*_\mathrm{f}(t), \tilde{x}^*_\mathrm{y}(t) \to 1$ and $\tilde{h}^*(\xi, t) \to E(\xi)$ in the limit $t \to \infty$. Fig. 8 show $\tilde{x}^*_\mathrm{f}$, $\tilde{x}^*_\mathrm{y}$ and $\tilde{h}^*$ plotted as a function of time for $B = 1$. It is readily observed that the numerics do rapidly approach this asymptotic value confirming our analysis.

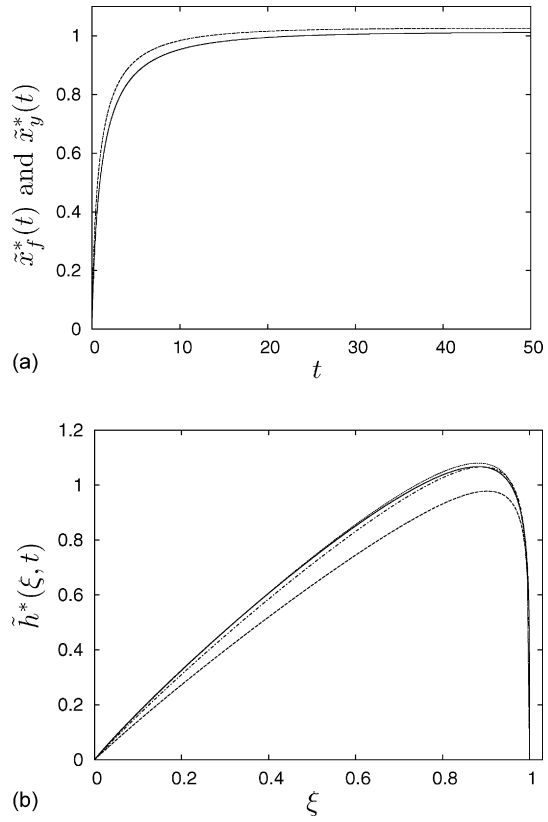

Fig. 8. Numerical results for $B = 1$. (a) The scaled front, x_f^*, (solid line) and yield, x_y^*, (dashed line) positions. (b) The rescaled spatial perturbation approaching the analytical solution of $E(\xi)$ (solid line) for dimensionless times $t = 5$ (−−), 15 (·–), 50 (· · ·).

6. Summary and discussion

In this article we have developed a 'lubrication' style model for the dam break of a viscoplastic fluid that flows solely under the force of gravity, modelling the rheology using a Herschel–Bulkley constitutive relation. The important dimensionless parameter in such systems is the Bingham number, B, which is the ratio of yield stress relative to the stresses generated by the weight of the flowing layer. In such motion there exists a profile in which the gravitational forces are balanced exactly by the yield stress of the fluid and under the assumption of negligible inertia, $Re \approx O(1)$, any initial condition will approach this arrested state. We have demonstrated that such an arrested state is not reached in finite time but is in fact approached asymptotically as $1/t^n$, where n is the power law index of the fluid.

We have investigated both numerically and analytically the two fundamentally different cases of $B < 1/3$ and $B \geq 1/3$ and found good agreement between the perturbation theory and numerical results. It has been possible to find how the front position, yield point (for $B \geq 1/3$) and height profile approach the arrested state and the dependance of this approach on the Bingham number, B, and power law index, n. Additionally, for the special case of a Bingham fluid ($n = 1$), we have been able to elucidate the perturbations to the final state analytically.

It is interesting to contrast this situation with that of Poiseuille or Couette flow of a yield stress fluid. In both these cases, when the driving pressure gradient or boundary velocity is reduced to zero the fluid arrests in finite time [23–25]. The reason for the different behaviour is that for our case of gravity driven flow, the force driving the motion never vanishes, but asymptotically approaches zero.

Our study has many applications both in industry and geophysics. For example measuring the consistency of common industrial slurries (such as concrete) and food purees [19]. There are many areas that warrant further study. For instance how is the asymptotic approach changed when the angle of inclination of the plane is nonzero? How do the effects of inertia modify the motion? Furthermore it would be interesting to conduct experimental investigations of the flows and their approach to the arrested state. Some observations have been made to suggest that such flows stop abruptly and do not asymptotically approach an arrested state [26]. This could be the hallmark of behaviour not captured by the Herschel–Bulkley constitutive relation and further investigation would be useful.

Acknowledgements

G.P. Matson acknowledges the financial support of NERC Environmental Mathematics and Statistics program. N.J. Balmforth and R.V. Craster are also thanked for many fruitful discussions.

Appendix A. Finite difference scheme

The flow occurs within the domain $0 \leq \xi \leq 1$ and we divide this range up into a grid of n equally spaced points with spacing $\delta\xi$. We discretize the spatial derivatives using a second order, centred difference scheme,

$$\frac{\partial h(\xi,t)}{\partial \xi} = \frac{h(\xi+\delta\xi,t) - h(\xi-\delta\xi,t)}{2\delta\xi} + O(\delta\xi^2),$$
$$\frac{\partial^2 h(\xi,t)}{\partial \xi^2} = \frac{h(\xi+\delta\xi,t) - 2h(\xi,t) + h(\xi-\delta\xi,t)}{\delta\xi^2} + O(\delta\xi^2).$$

To make the time derivative second order in δt we use a half step scheme. The governing equation, (4.6), can be simply written as

$$\frac{\partial h(\xi,t)}{\partial t} = F[h(\xi,t)], \tag{A.1}$$

where $F[h(\xi,t)]$ is a functional that is equal to the right hand side of (4.6). The time stepping scheme can now be written as a two step process involving first, a half step, followed by the full step using one sided time derivatives.

$$h(\xi, t+\delta t/2) = h(\xi,t) + \frac{\delta t}{2} F[h(\xi,t)] + O(\delta t), \tag{A.2}$$

$$h(\xi, t+\delta t) = h(\xi,t) + \delta t F[h(\xi, t+\delta t/2)] + O(\delta t^2). \tag{A.3}$$

Using this scheme an iteration is made across all the interior points, $0 < \xi < 1$. We fix the height at the front by insisting it must vanish. If $x_y > 0$ we simply fix the height at $\xi = 0$ to be unity. If however $x_y = 0$ the height at the back is no longer unity and must be fixed using (4.5),

$$h(0,t) = \sqrt{h(\delta\xi,t)^2 + 2Bx_f\delta\xi + O(\delta\xi^2)}. \tag{A.4}$$

In order to track x_y we must apply (4.7) to obtain $\dot{x}_y$. The point $\xi = 0$ is a discontinuity in the height profile and hence we use one sided derivatives here with our knowledge that $h(0,t) = 1$,

$$\frac{\partial h(0,t)}{\partial \xi} = \frac{4h(\delta\xi,t) - h(2\delta\xi,t) - 3}{2\delta\xi} + O(\delta\xi^2),$$
$$\frac{\partial^2 h(0,t)}{\partial \xi^2} = \frac{h(2\delta\xi,t) - 2h(\delta\xi,t) + 1}{\delta\xi^2} + O(\delta\xi^2).$$

With the knowledge of $\dot{x}_y$ we can apply a first order time derivative to calculate the new yield position,

$$x_y(t+\delta t) = x_y(t) + \dot{x}_y\delta t + O(\delta t). \tag{A.5}$$

When the yield point reaches the back wall we force $x_y = 0$ and $\dot{x}_y = 0$ for all subsequent time steps.

The profile must also satisfy conservation of volume and this is implemented using (4.8) to find $x_a(t+\delta t)$ and hence by using the previous value it is possible to find $\dot{x}_a$ using a first order backwards derivative,

$$\dot{x}_a = \frac{x_a(t+\delta t) - x_a(t)}{\delta t} + O(\delta t). \tag{A.6}$$

The asymptotic flow profile has a singularity at the front caused by the gradient becoming infinite. This will cause problems with estimating the gradient at the nose so we make the change of variable $\hat{h}(\xi,t) = h(\xi,t)^2$. In these coordinates the asymptotic behaviour of the nose is no longer singular but behaves linearly as $\xi \to 1$. The integral of the profile is obtained by using the Trapezium Rule in the new variables ($\hat{h}$ and ξ). The changes of variable to $h \to \hat{h}$ and $x \to \xi$ are simply used as convenient tools, all of the results will be given in terms of the original variables h and x.

References

[1] G. Hulme, The interpretation of lava flow morphology, Geophys. J. R. Astronom. Soc. 39 (1974) 361–383.
[2] D.I. Osmond, R.W. Griffiths, The static shape of yield strength fluids slowly emplaced on slopes, J. Geophys. Res. 106 (B8) (2001) 16241–16250.
[3] P. Coussot, S. Proust, Slow, unconfined spreading of a mudflow, J. Geophys. Res. 101 (B11) (1996) 25,217–25,229.
[4] X. Huang, M.H. Garcia, A Herschel–Bulkey model for mud flow down a slope, J. Fluid Mech. 374 (1998) 305–333.
[5] K.F. Liu, C.C. Mei, Slow spreading of a sheet of Bingham fluid on an inclined plane, J. Fluid Mech. 207 (1989) 505–529.
[6] S.D.R. Wilson, S.L. Burgess, The steady, spreading flow of a rivulet of mud, J. Non-Newtonian Fluid Mech. 79 (1998) 77–85.
[7] H.E. Huppert, The propagation of two-dimensional and axisymmetric viscous gravity currents over a rigid horizontal surface, J. Fluid Mech. 121 (1982) 43–58.
[8] J.R. Lister, Viscous flows down an inclined plane from point and line sources, J. Fluid Mech. 242 (1992) 631–653.
[9] N.J. Balmforth, R.V. Craster, Geophysical aspects of non-Newtonian fluid mechanics, in: N.J. Blamforth, A. Provenzale (Eds.), Geomorphological Fluid Mechanics, Lecture Notes in Physics, Gran Combin Summer School, Springer, 2002, pp. 34–51.

[10] N.J. Balmforth, R.V. Craster, A consistent thin-layer theory for Bingham plastics, J. Non-Newtonian Fluid Mech. 84 (1999) 65–81.
[11] A. Ritter, Die Fortpflanzung der Wasserwellen, Z. Vereines Deutsch. Ing. 36 (33) (1892) 947–954.
[12] G.B. Whitham, The effects of hydraulic resistance in the dambreak problem, Proc. R. Soc. Lond. A 227 (1955) 399–407.
[13] A.J. Hogg, D. Pritchard, The effects of hydraulic resistance on dam-break and other shallow inertial flows, J. Fluid Mech. 501 (2004) 179–212.
[14] N.J. Balmforth, R.V. Craster, R. Sassi, Shallow viscoplastic flow on an inclined plane, J. Fluid Mech. 470 (2002) 1–29.
[15] Q.D. Nguyen, D.V. Boger, Measuring the flow properties of yield stress fluids, Annu. Rev. Fluid Mech. 24 (1992) 47–88.
[16] N. Pashias, D.V. Boger, J. Summers, D.J. Glenister, A fifty cent rheometer for yield stress measurements, J. Rheol. 40 (6) (1996) 1179–1189.
[17] W.R. Schowalter, G. Christensen, Toward a rationalization of the slump test for fresh concrete: comparisons of calculstions and experiments, J. Rheol. 42 (4) (1998) 865–870.
[18] P. Perona, Bostwick degree and rheological properties: an up-to-date viewpoint, Appl. Rheology 15 (4) (2005) 218–229.
[19] N.J. Balmforth, R.V. Craster, P. Perona, A. Rust, R. Sassi, The Bostwick consistometer and viscoplastic dam breaks, J. Non-Newtonian Fluid Mechanics, in press.
[20] P. Coussot, J.M. Piau, On the behavior of fine mud suspensions, Rheol. Acta 33 (1994) 175–184.
[21] N. Didden, T. Maxworthy, The viscous spreading of plane and axisymmetric gravity currents, J. Fluid Mech. 121 (1982) 27–42.
[22] J. Gratton, F. Minotti, Theory of crepping gravity currents of a non-newtonian liquid, Phys. Rev. E 60 (6) (1999) 6960–6967.
[23] R.R. Huilgol, B. Mena, J.M. Piau, Finite stopping time problems and rheometry of Bingham fluids, J. Non-Newtonian Fluid Mech. 102 (2002) 97–107.
[24] R.R. Huilgol, Z. You, Application of the augmented Lagrangian method to steady pipe flows of Bingham, Casson and Herschel–Bulkley fluids, J. Non-Newtonian Fluid Mech. 128 (2005) 126–143.
[25] M. Chatzimina, G.C. Georgiou, I. Argyropaidas, E. Mitsoulis, R.R. Huilgol, Cessation of Couette and Poiseuille flows of a Bingham plastic and finite stopping times, J. Non-Newtonian Fluid Mech. 129 (2005) 117–127.
[26] C. Ancey, H. Jorrot, Yield stress for particle suspensions within a clay dispersion, J. Rheol. 45 (2001) 297–319.